

# Safety Evaluation of Low-Rise Steel Structures under Wind Loads by Nonlinear Database-Assisted Technique

Dat Duthinh<sup>1</sup> and William P. Fritz<sup>2</sup>

**Abstract:** The design of a large proportion of the low-rise metal buildings in the United States is based on the ASCE 7-93 Standard and the use of allowable stress design (ASD). In this paper we examine, for a typical case, the question of whether such buildings satisfy requirements implicit in more recent versions of the ASCE Standard. We base our investigation into this question on all three wind loading conditions specified in the ASCE 7-02 Standard. In particular, we use the nonlinear database-assisted design technique to assess the degree of safety of a typical portal frame belonging to the wind-force resisting system of a low-rise industrial structure designed in accordance with ASCE 7-93 and ASD. The conclusion of our assessment is that the frame being considered satisfies all ASCE 7-02 requirements with respect to wind loading, but that its safety level is relatively low, and could be improved substantially at very low cost.

**DOI:** 10.1061/(ASCE)0733-9445(2007)133:4(587)

**CE Database subject headings:** Allowable stress design; Steel structures; Structural design; Databases; Nonlinear analysis; Ultimate strength; Wind loads.

## Introduction

The design of a large proportion of low-rise buildings in the United States is based on the ASCE 7-93 Standard (ASCE 1993) and the use of allowable stress design (ASD) (AISC 1989). This is the case in part because a large investment has been made by trade organizations into software based on such designs. In this paper we examine, for a typical case, the question of whether such buildings satisfy requirements implicit in more recent versions of the ASCE Standard. We base our investigation into this question on all three wind loading conditions specified in the ASCE 7-02 Standard (2003). In particular, we use the nonlinear database-assisted design technique to assess the degree of safety of a typical portal frame belonging to the wind-force resisting system of a low-rise industrial structure designed in accordance with the ASCE 7-93 Standard and ASD.

Elements of the nonlinear, database-assisted design method used in this paper were developed by Jang et al. (2002) for low-rise buildings subjected to wind loads. The method consists of using databases of pressures measured in wind tunnel tests, as allowed by ASCE 7-02, Sect. 6.6.2, Item 3. In addition, the method uses these pressures in nonlinear analyses yielding estimates of nominal ultimate capacities of the structure—hence the name nonlinear database-assisted design (NLDAD). Unlike

Jang et al. (2002), the approach used in this paper targets all potentially critical cross sections of the structure being designed.

To illustrate the method, we investigate one frame of a steel warehouse originally designed to satisfy ASCE 7-93 wind loads and ASD requirements. Such an investigation is warranted by the fact that numerous low-rise buildings subjected to wind loads experience failure not only of components such as purlins, for example, but of wind-force resisting systems as well (see, e.g., Simiu and Miyata 2006, p. 127). We seek to ascertain the degree to which the frame is adequate in safety level terms. The nonlinear behavior is investigated by using a detailed finite-element analysis into the large displacement, postyielding range, with account taken of local plate buckling and initial imperfections. Results, structural performance improvements, and the margin of safety invoked in ASCE 7-02 Commentary are then discussed.

## Structure

The structure analyzed is a preliminary design of a low-rise steel warehouse by Ceco Building Systems, which used standard software based on ASCE 7-93 Standard and ASD, for the coastal region near Miami. The building dimensions are 100 ft (30.5 m) in width  $\times$  200 ft (61 m) in length  $\times$  22 ft (7.2 m) in height with the gable roof rising from an eave height of 20 ft (6.1 m) at a slope of 1/24. The roof and the walls are supported by nine frames that span the width of the building and are spaced 25 ft (7.62 m) apart (Fig. 1). The frames are connected to each other by longitudinal girts, purlins (Fig. 2), and braces (below the rafter or roof part of the frame). The girts on the columns are spaced between 4 ft 4 in. (1.32 m) and 4 ft 10 in. (1.47 m) apart; most of the purlins on the top of the rafter are spaced 4 ft 1 1/16 in. (1.25 m) apart, and the braces below the roof are 6 ft (1.83 m) apart.

The example frame analyzed here is adjacent to the end frame (F2 in bold in Fig. 1), and is of welded plate construction, with an I-cross section (Fig. 3). The columns consist of two flanges 8 in.  $\times$  0.375 in. (203 mm  $\times$  9.5 mm) connected by a web

<sup>1</sup>Building and Fire Research Laboratory, National Institute of Standards and Technology, Gaithersburg, MD 20899-8611. E-mail: dduthinh@nist.gov

<sup>2</sup>Building and Fire Research Laboratory, National Institute of Standards and Technology, Gaithersburg, MD 20899-8611. E-mail: wfritz@nist.gov

Note. Associate Editor: Kurtis R. Gurley. Discussion open until September 1, 2007. Separate discussions must be submitted for individual papers. To extend the closing date by one month, a written request must be filed with the ASCE Managing Editor. The manuscript for this paper was submitted for review and possible publication on June 9, 2005; approved on August 28, 2006. This paper is part of the *Journal of Structural Engineering*, Vol. 133, No. 4, April 1, 2007. ©ASCE, ISSN 0733-9445/2007/4-587-594/\$25.00.

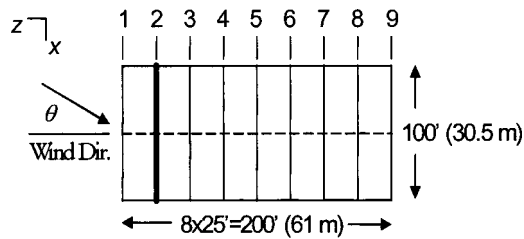


**Fig. 1.** Plan view of typical frame layout (F1–F9) and wind directions ( $\theta$ ). Location of the selected frame (F2) is in bold and the centerline is shown (dashed line)

0.25 in. (6.4 mm) thick ranging in depth from 10 in. (254 mm) to 47 in. (1194 mm). The rafter consists of two flanges 6 in. (152 mm) wide of thickness varying from 0.625 in. (15.9 mm) to 0.25 in. (6.4 mm). They are connected by a web of depth varying from 42 in. (1067 mm) at the haunches (S1 and S5, Fig. 2), where it meets the columns, to 25 in. (635 mm) at the pinches or shallowest parts (S2 and S4). The rafter web thickness varies from 0.25 in. (6.4 mm) at the haunch to 0.149 in. (3.8 mm) at the ridge, or top (S3). Vertical stiffeners are located at the haunches (S1 and S5) and the ridge (S3).

### ASCE Wind Loads

According to ASCE 7-02, the design wind pressures  $p$  for the main wind force-resisting system is given by [ASCE 7-02, Eq. (6.17)]

$$p = qGC_p - q_i(GC_{pi})$$

where  $C_p$  = external pressure coefficient;  $GC_{pi}$  = internal pressure coefficient;  $G$  = gust effect factor; and  $q$ ,  $q_i$  = external, internal wind pressures.

The wind pressure at height  $y$  is evaluated from [see ASCE 7-02 Eq. (6.15)]

$$q_y = (\rho/2)K_yK_zK_dV^2I$$

where  $\rho/2$  = coefficient (0.00256 lbf/ft<sup>2</sup> or 0.613 N/m<sup>2</sup>) corresponding to half of the mass density of air,  $I$  = importance factor,  $K_d$  = wind directionality factor,  $K_y$  = velocity pressure coefficient,  $K_z$  = topographic factor, and  $V$  = basic wind speed [nominal design 3 s gust wind speed at 33 ft (10 m) above ground for Exposure C]; for the Miami coastal region,  $V = 140$  mi/h (62.6 m/s). In this case, the velocity pressure evaluated at eave height is:

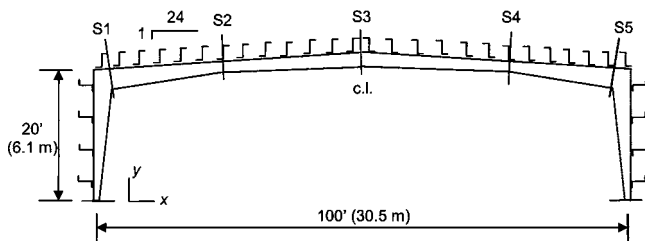


**Fig. 2.** Schematic of a typical frame at full scale. Moments are calculated at the five sections shown (S1–S5). Structure is symmetric about the centerline (c.l.). Braces below rafters are not shown.

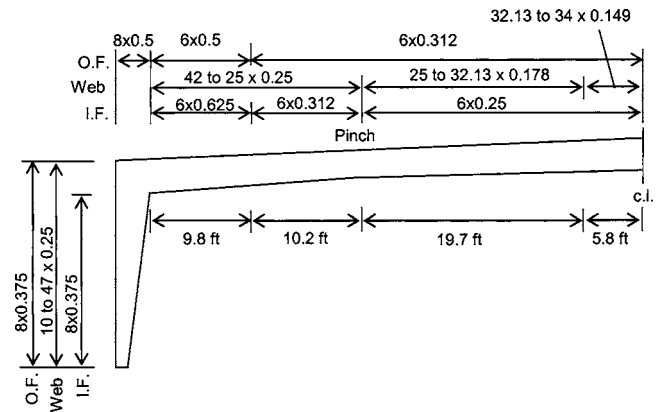


**Fig. 3.** Typical frame section. Dimensions of outside flange (O.F.), web and inside flange (I.F.) are given as width (depth) by thickness in inches (1 in. = 25.4 mm, 1 ft = 304.8 mm).

$$q_h = 0.00256 \times 0.90 \times 1.0 \times 0.85 \times 140^2 \times 1.0 = 38.38 \text{ psf or } 1,838 \text{ Pa}$$

For “base load cases for low-rise walls and roofs of enclosed or partially enclosed buildings” (ASCE 7-02 Fig. 6-10), the external pressure coefficients for the left column (surface 1), left half of roof (2), right half of roof (3), and right column (4) are  $GC_{pf} = 0.40, -0.69, -0.37,$  and  $-0.29$ , respectively, where positive pressures act into the surface. When multiplied by  $q_h$ , these coefficients give the external velocity pressures,  $q_h GC_{pf} = (15.35, -26.49, -14.20,$  and  $-11.23)$  psf or (735,  $-1268, -680,$  and  $-538)$  Pa for surfaces 1, 2, 3, and 4, respectively. These pressures are scaled by 25 ft/flange width (7.62 m/flange width) to account for the roof and wall tributary width supported by each frame, and then they are applied to the model. We note that the pressures of ASCE 7-02 Fig. 6-10 are referred to in the Commentary of the Standard (p. 286, Column 2) as “pseudopressures,” as rather than representing actual physical pressures that would act on the building in wind they are very simplified representations of such pressures, adopted because they are suitable for incorporation in tables and graphs.

For enclosed buildings, ASCE 7-02 Fig. 6.5 gives internal pressure coefficient  $GC_{pi} = \pm 0.18$ , which produces  $q_i GC_{pi} = \pm 38.38 \text{ psf} \times 0.18 = \pm 6.908 \text{ psf}$  (331 Pa). These pressures are scaled as previously before application to the model. As the external wind pressure tends to lift the roof, the more demanding load combination is for an internal pressure acting outward, whose effect adds to that of the external pressure.

Of the basic load combinations specified in ASCE 7-02 Sect. 2.3, the following combination was selected as the most critical: 0.9 dead load +  $\lambda$  wind load, with  $\lambda = 1.6$ . As both external and internal wind pressures tend to lift the roof, gravity has a beneficial effect, and thus the load combination with the highest wind and the lowest dead load is the most demanding. According to the building manufacturers, the roof dead load is 2.03 psf (97 Pa). Load Case 1 (LC1) is therefore 0.9 dead load +  $\lambda$  ASCE wind loads, where the wind load factor  $\lambda$  is a measure of the building wind resistance. Note that, for the case under consideration in this paper, the wind pressures determined in accordance to Fig. 6-10 of ASCE 7-02 (Method 2b) represent a refinement of, and tend to be lower than, the pressures specified in Fig. 6-6 of ASCE 7-02 (Method 2a) multiplied by a gust factor. The pressures of Fig. 6-6 of ASCE 7-02 are in turn lower than the

**Table 1.** Maximum and Minimum Bending Moments at Five Sections of Frame F2

Wind direction $\theta$ (degrees)	Section S1		Section S2		Section S3		Section S4		Section S5	
	Max	Min	Max	Min	Max	Min	Max	Min	Max	Min
(a) kip ft										
0	929.1	59.4	145.4	-107.7	-15.2	-283.6	137.9	-122.0	934.6	72.0
10	916.2	100.7	114.6	-98.6	-27.7	-290.0	125.5	-98.4	<b>943.7</b>	75.3
20	905.1	108.8	138.2	-88.4	-31.6	-298.2	107.3	-123.7	913.8	86.5
30	885.0	76.9	<b>196.2</b>	-61.9	-16.9	-294.6	93.0	<b>-175.7</b>	905.6	33.3
40	<b>984.1</b>	67.2	169.2	-44.2	-4.4	<b>-306.6</b>	69.0	-153.4	930.4	<b>-65.2</b>
50	717.6	58.3	152.4	-76.5	-9.3	-236.7	65.6	-133.3	672.6	1.3
60	729.9	23.5	124.6	-104.3	7.6	-195.6	96.1	-114.5	584.1	-24.0
70	703.3	<b>17.7</b>	76.0	<b>-162.5</b>	<b>8.0</b>	-190.3	<b>151.5</b>	-69.0	611.9	-26.8
80	618.1	22.3	38.3	-135.1	4.9	-156.9	136.0	-38.1	523.0	-11.9
90	667.6	46.5	24.2	-150.7	-2.7	-180.2	142.3	-24.9	579.1	17.4
(b) kN m										
0	1259.8	80.6	197.1	-146.0	-20.6	-384.5	187.0	-165.4	1267.3	97.6
10	1242.3	136.5	155.4	-133.7	-37.6	-393.3	170.2	-133.4	<b>1279.6</b>	102.1
20	1227.3	147.6	187.4	-119.9	-42.9	-404.3	145.5	-167.8	1239.1	117.3
30	1200	104.3	<b>266.0</b>	-83.9	-22.9	-399.5	126.1	<b>-238.2</b>	1228	45.1
40	<b>1334.5</b>	91.1	229.4	-59.9	-6.0	<b>-415.8</b>	93.6	-208.0	1261.6	<b>-88.4</b>
50	973.1	79.0	206.6	-103.7	-12.6	-320.9	88.9	-180.7	912.0	1.8
60	989.7	31.8	169.0	-141.4	10.3	-265.3	130.3	-155.3	792.0	-32.5
70	953.7	<b>24.0</b>	103.0	<b>-220.3</b>	<b>10.9</b>	-258.0	<b>205.4</b>	-93.5	829.8	-36.3
80	838.2	30.3	52.0	-183.2	6.6	-212.8	184.4	-51.7	709.2	-16.1
90	905.2	63.0	32.8	-204.4	-3.7	-244.3	193.0	-33.7	785.2	23.6

pressures specified in ASCE 7-93. Therefore, for buildings designed in accordance with ASD, designs based on ASCE 7-93 tend to be conservative in relation to designs based on ASCE 7-02 Figs. 6-6 and 6-10. This fact is verified by the detailed calculations that follow. In addition to the pressures given by Figs. 6-6 and 6-10, an ASCE 7-02 provision (Sect. 6.6.2, Item 5) allows the use of pressures obtained in the wind tunnel (Method 3). The use of NLDAD is based on this provision, and provides a useful measure of the safety level of buildings subjected to wind loads, as is shown subsequently in this paper.

## Wind Tunnel Tests

A 1/200 model was tested at the University of Western Ontario under open terrain conditions (Lin and Surry 1997). Pressure taps covering tributary areas of typical (prototype) dimensions 6.7 ft (2.04 m)  $\times$  8.33 ft (2.54 m, z) on the roof, 5.0 ft

(1.52 m, y)  $\times$  8.33 ft (2.54 m, z) on the sidewalls and 6.67 ft (2.03 m, x)  $\times$  5.0 ft (1.52 m, y) on the end walls recorded external pressures at a (model) frequency of 400 Hz for about 60 s (model time) or 1 h (prototype time). The wind tunnel pressures, normalized to a wind speed of 1 ft/s (0.305 m/s) at eave height, were multiplied by a load factor  $\lambda$  times the square of a reference wind velocity measured by an hourly gust speed  $V_{h,20}$  = 86 mi/h (38.4 m/s) at 20 ft (6.1 m), the eave height above open terrain. This wind speed corresponds to the 3 s gust speed  $V_{3s,33}$  = 140 mi/h (62.6 m/s) at 33 ft (10 m) elevation from the ASCE 7-02 Standards for the Miami coastal region, as established by ASCE 7-02 Commentary, Fig. C6-2, and Simiu and Scanlan (1996)

$$\frac{V_{h,20}}{V_{3s,33}} = \frac{V_{h,33} V_{20}}{V_{3s,33} V_{33}} = \frac{1}{1.52} \left( \frac{20}{33} \right)^{1/7} = 0.613 \quad (1)$$

In this analysis, pressure time histories covering wind incidence from 0 to 90° were read at 10° intervals, and moments were

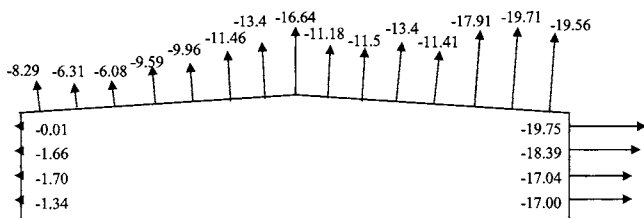


**Fig. 4.** External wind forces (kN) for LC2 that create maximum bending moment M1 at Section S1 for wind direction 40° (1 kip = 4.448 kN)

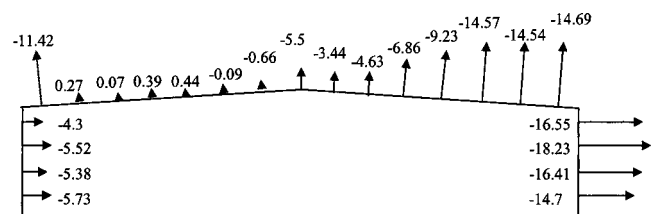


**Fig. 5.** External wind forces (kN) for LC3 that create maximum bending moment M2 at Section S2 for wind direction 30° (1 kip = 4.448 kN)

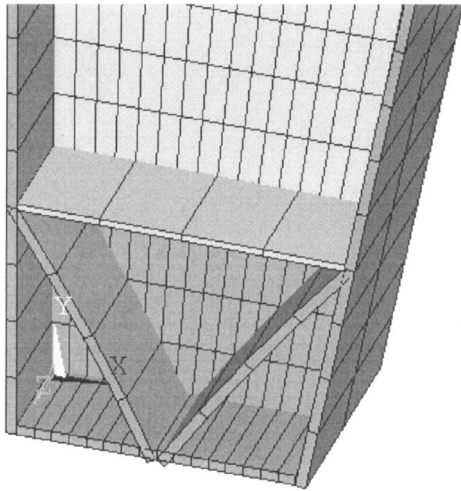


**Fig. 6.** Base plate and triangular stiffener at support

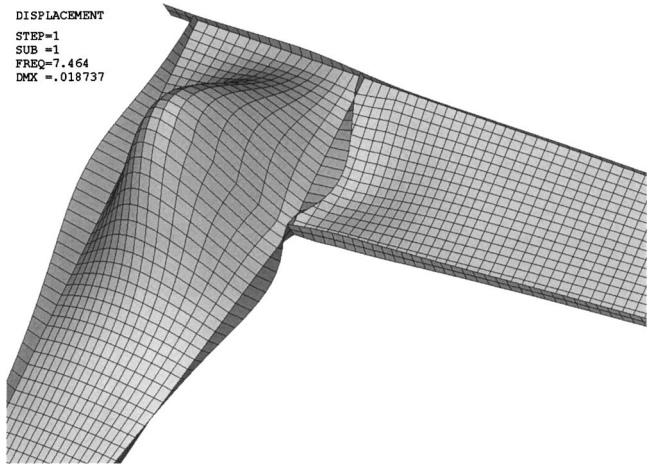


**Fig. 7.** Initial deformation of left haunch (highly exaggerated). Similar initial deformation of right haunch is also used.

calculated at five sections (S1-S5, Fig. 2) deemed critical, namely the two haunches, two pinches and the ridge, using a linear model. The capability to use wind pressures from databases and compute moments by simple linear analysis was first developed in the *Wind Load Design Environment for Low-Rise Structures* (WILDE-LRS, Whalen et al. 2000).

To determine the load cases (wind direction and time) to be investigated further, the minimum and maximum of these moments *over time* for winds blowing from each direction were

selected (Table 1). These peak moments, which, in general, occur at different times, were used only for load case selection, and not for the detailed, nonlinear structural analysis. Next, for each section, the highest maximum and the lowest minimum *over all wind directions* were chosen (in bold type). If these extreme peaks have the same sign, as is the case for S1, then the peak with the higher absolute value was selected. For S3 and S5, the peaks are of different signs, but more than one order of magnitude different, so only the higher absolute value was considered.

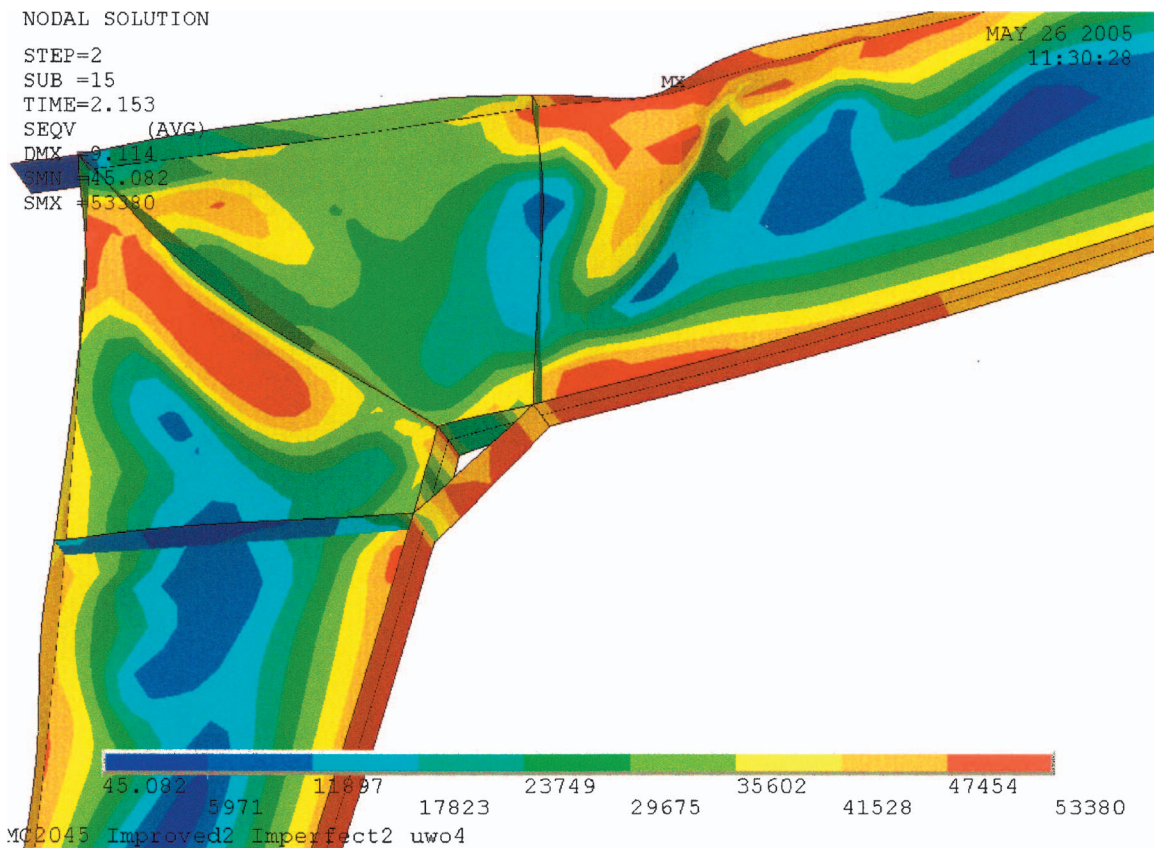


**Fig. 8.** (Color) Left haunch of initially imperfect structure  $B_i$  under LC2. Von Mises stresses in psi (1 psi=6,895 Pa) at ultimate  $\lambda=2.143$ . Maximum deflection=9.11 in. (231 mm).

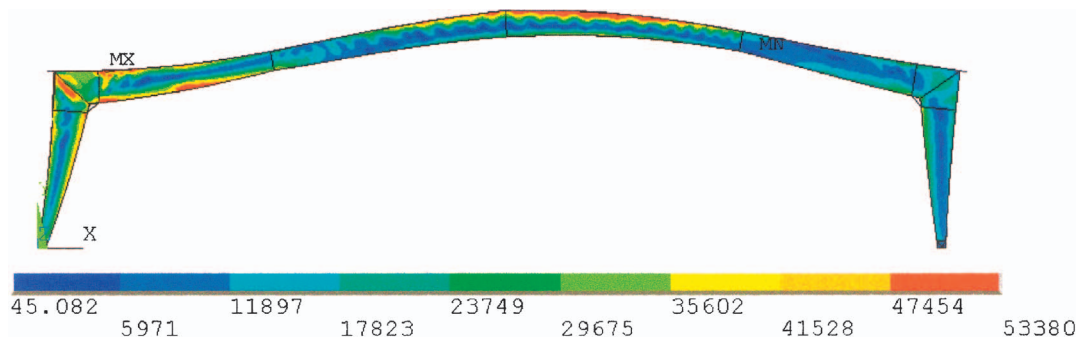


**Fig. 9.** (Color) Initially imperfect structure  $B_1$  under LC2. Von Mises stresses in psi (1 psi=6,895 Pa) at ultimate  $\lambda=2.143$ . Maximum deflection=9.11 in. (231 mm).

Symmetry was then invoked to further reduce the number of load cases: the case  $M1=984.1$  kip ft (1,334.5 kN m) was preferred over  $M5=943.7$  kip ft (1,279.6 kN m), where  $M1$  is the *maximum* moment at section S1; likewise, the case  $M2=196.2$  kip ft (266 kN m) was selected over  $M4=151.5$  kip ft (205.4 kN m). The case  $M2=196.2$  kip ft (266 kN m) occurred for a wind incidence of  $30^\circ$ , which is also the direction that caused  $M4=-175.7$  kip ft (-238.2 kN m), where  $m4$  refers to the *minimum* moment at section S4. Although these two cases occurred at different times, the two pressure distributions were similar, and only case  $M2=196.2$  kip ft (266 kN m) needed to be selected. Wind direction  $40^\circ$  caused  $m3=-306.6$  kip ft (-415.8 kN m) and also  $M1=984.1$  kip ft (1,334.5 kN m). Again, the two pressure distributions, although occurring at different times, were similar, and only one case needed to be selected.

This example illustrates how WiLDE-LRS can be used to define the design envelope. Careful selection of load cases allows consideration of *all* critical sections and alleviates the amount of computation required in the detailed design. In the end, only two load cases, shown in Figs. 4 and 5, were needed. They correspond to wind directions  $40$  and  $30^\circ$  and cause the instantaneous peak moments  $M1$  and  $M2$ , respectively. Load case 2 (LC2) and load case 3 (LC3) combine  $\lambda$  times the external wind forces shown in Figs. 4 and 5 with  $\lambda$  times the ASCE internal wind forces and 0.9 times the dead load.

### Finite-Element Model

The model used 11,000 shell finite-elements, the great majority of which have a typical dimension of 3 in. (76 mm). The element, ANSYS Shell 181, has four corner nodes with six degrees of freedom each. Full integration was performed on web elements, whereas reduced integration was used on flange elements where deformation was mostly out-of-plane. The model is three dimensional in the sense that all six degrees of freedom are considered, but as only one frame is analyzed, the purlins, girts, and braces are modeled as constraints to the  $z$  (out-of-plane) translation. Also, the two ground supports of the frame are modeled as hinges, with rotation about  $z$  allowed. Point supports cause considerable stress concentration, local yielding and distortion, and numerical difficulty at relatively small loads. Thus, a base plate and triangular stiffener were added to the frame at each support (Fig. 6), a realistic improvement that is recommended for future designs. This strengthening and stiffening of the supports are the only differences between structure A and the actual structure.

Another location with high stress concentration is the internal corner between column and rafter (called the haunch). To alleviate this concentration, structure B was created with a short oblique member (0.375 in. or 9.5 mm thick) and horizontal, vertical and diagonal stiffeners that allowed an alternative load path

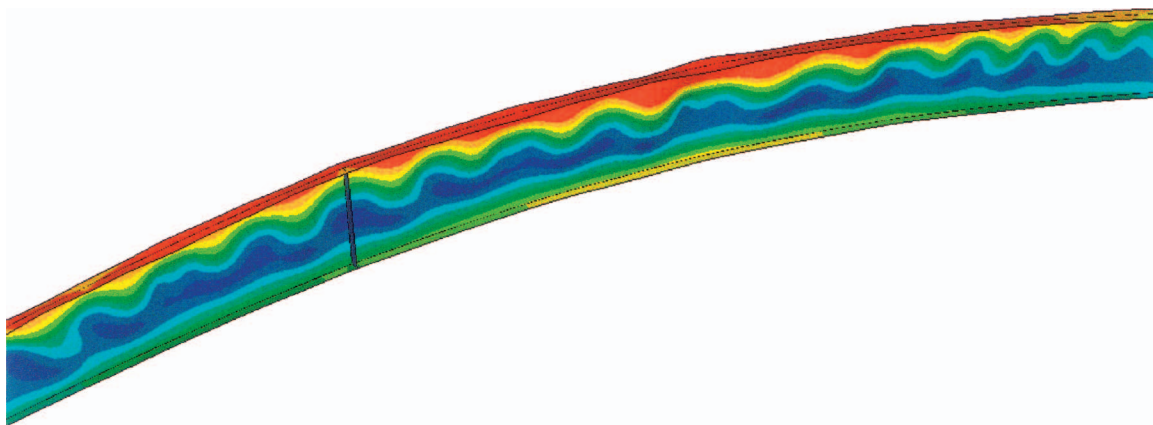


**Fig. 10.** (Color) Ridge of initially imperfect structure  $B_1$  under LC2. Von Mises stresses in psi (1 psi=6,895 Pa, same color scale as in Fig. 9) at ultimate  $\lambda=2.143$ . Maximum deflection=9.11 in. (231 mm).



**Fig. 11.** Initial deformation of web and flanges at right pinch, top view (highly exaggerated). Similar initial deformation of left pinch is also used

at this location. The haunches of structures A and B are shown in Figs. 7 and 8. In addition, as the governing load cases caused the roof to lift, forcing web and flange local buckling at the ridge, structure B switched the thicker flange from the tension (top) to the compression (bottom) side of the rafter, and kept the web thickness at 0.178 in. (4.5 mm), rather than reducing it to 0.149 in. (3.8 mm) in the ridge region. Finally, web stiffeners were added at the pinches, while the same support strengthening details as in structure A were kept. These structural improvements only increased the weight by 3.6%.

The material used in the model was steel, with a modulus of elasticity of 29,000 ksi (200 GPa), a yield strength of 50 ksi (344 MPa) and an ultimate strength of 65 ksi (448 MPa), similar to the actual design material. The gradual stress-strain curve beyond yield is described by the Voce model

$$\sigma = \sigma_y + E_t \varepsilon_p + R(1 - \exp(-b\varepsilon_p)) \quad (2)$$

where  $b$ =material constant=20;  $E_t$ =tangent modulus=0;  $R$ =material constant=15 ksi (103 MPa);  $\sigma$ =stress;  $\sigma_y$ =yield stress; and  $\varepsilon_p$ =plastic strain.

## Nonlinear Analysis

In a first step, gravity was applied with a factor of 0.9, and the structure analyzed. In the second step, wind load was applied in incremental fashion until the structure failed. The criterion for failure is excessive element distortion resulting in the structural analysis program being unable to converge to a solution, even after repeated halving of load increments. Numerical instability had to correspond to actual physical imminent collapse as seen from significant local buckling and/or section yielding (Figs. 8–10) before attempts at restarting the program were abandoned.

As local buckling played an important role in the ultimate strength of the structure, a second series of analysis was performed that accounted for initial imperfections. For local plate buckling, the relevant dimensions are width and thickness, not length. Most plates in the frame have a width to thickness ratio of about 200, and a realistic, but severe, initial out-of-plane deformation amplitude of 1% of width, or 0.3 in. (7.6 mm) was selected. Initial deformations were obtained from linear combinations of (linear) eigenvalue buckling modes. As linear and nonlinear buckling of initially perfect structures do not necessarily result in buckles at the same places, a series of elementary loads were used to force the frame to buckle (linearly) at the same critical locations as in the nonlinear, initially perfect, buckling analysis. As the severe initial imperfections had their maximum



**Fig. 12.** Initial deformation of web and flanges at ridge, top view (highly exaggerated).

**Table 2.** Wind Load Factor  $\lambda$  at Ultimate Strength

Structure	ASCE 7-02 (subscript 1)	LC2 (subscript 2)	LC 3 (subscript 3)	Weight [lbf (kN)]
$A_p$ perfect	1.938	2.115	2.916	5,357(23.83)
$B_p$ perfect	2.231	2.510	3.171	5,549(24.68)
$A_i$ imperfect	1.642	1.743	2.273	
$B_i$ imperfect	2.076	2.143	2.801	

amplitudes at these critical sections, they represented a worst case. Figs. 7, 11, and 12 show the elementary buckles, under gravity, negative gravity (up), two point loads at the pinches (one up and one down), that were combined to form the imperfect frame. Where initial deformations consist of left-right symmetrical pairs, only one half of each pair is shown (Figs. 7 and 11). The nonlinear analysis then proceeded in the same way as for the initially perfect frame.

## Results

Under LC1 (ASCE 7-02), structure A buckled at the web in the region of the ridge, whereas Structure B buckled at the left haunch. By delaying buckling of the rafter web, the structural modifications from A to B mobilized larger areas of the rafter and left column, and also alleviated the stress concentration at the corner. The more efficient structure resulted in higher wind resistance.

Under LC2, initially perfect structure,  $A_p$ , failed by a combination of yielding and local buckling at the ridge and left haunch. In contrast, Structure  $B_p$  failed by yielding, with little evidence of buckling. The initially imperfect structure,  $A_i$ , failed in a similar fashion to  $A_p$ , with more extensive buckling at the ridge and left haunch, whereas  $B_i$  failed by extensive buckling at the ridge, left haunch and adjacent regions. Results are shown in Von Mises stress contours on the deformed structure at ultimate (Figs. 8–10). The maximum deflection reported gives a measure of the deformation capacity of the structure before collapse.

Under LC3, structure  $A_p$  exhibited substantial yielding and moderate buckling at the pinches, and high stress concentration at the left haunch corner. In comparison, structure  $B_p$  exhibited extensive yielding near the pinches, but no buckling, and smaller stresses at the left haunch corner. Structure  $A_i$  failed by buckling at the left haunch and rafter web near the right pinch, in the region of peak deflection. Structure  $B_i$  exhibited extensive buckling of the rafter web, and some buckling at the left haunch.

As mentioned earlier, the load combination applied was 0.9 dead load +  $\lambda$  wind load, where the wind load factor  $\lambda$  provides a measure of the building wind resistance. The same ASCE 7-02 internal wind pressure was used in all analyses. Table 2 lists the values of  $\lambda$  that correspond to the ultimate strength of the initially perfect and the initially imperfect structure A and its improved

**Table 3.** Percent Change due to Structural Modifications and Initial Imperfections

	ASCE 7-02	LC2	LC3	Weight
$100(B_p - A_p)/A_p$	15	19	8.7	3.6
$100(B_i - A_i)/A_i$	26	23	23	
$100(A_i - A_p)/A_p$	-15	-18	-22	
$100(B_i - B_p)/B_p$	-7.5	-15	-12	

**Table 4.** Percent Change between Using ASCE 7-02 and Load Case 2

Quantity	Change
$100(A_{p2}-A_{p1})/A_{p1}$	9
$100(B_{p2}-B_{p1})/B_{p1}$	13
$100(A_{i2}-A_{i1})/A_{i1}$	6
$100(B_{i2}-B_{i1})/B_{i1}$	3
$100(B_{p2}-A_{p1})/A_{p1}$	30
$100(B_{i2}-A_{i1})/A_{i1}$	31

version B for three load cases. The ultimate wind load factor  $\lambda$  for LC3 is always greater than for LC1 (ASCE 7-02) or LC2, and thus is not governing. It is remarkable that the  $\lambda$  values for LC1 and LC2 are close to each other, with LC1 being conservative, which confirms the validity of the ASCE wind pressures. All  $\lambda$ 's are greater than 1.6, the value specified by ASCE 7-02, and therefore the structure meets ASCE 7-02 Standards. This point will be revisited later.

Table 3 shows the relative change between various entries of Table 2. Significant improvement in wind resistance was achieved by structure B compared to structure A (between 15 and 26%), at the cost of an increase in weight of only 3.6%. The improvement in structural performance is more important in the presence of initial imperfections than in their absence. The second half of Table 3 confirms that improved structure B is less imperfection-sensitive than structure A. Table 4 shows the relative advantage of using LC2 over LC1. The gain in  $\lambda$  (or in maximum wind speed bearable) in going from ASCE wind pressures to the more accurate database-assisted design (DAD) ranges from 3 to 13%. Combining DAD with structural improvements that were partly enabled by nonlinear analysis, the so-called NLDAD leads to substantial improvements in wind resistance of 30%. Conversely, a decrease in weight of 10% or even more is possible with NLDAD, with no loss of structural capacity. As column 1 of Table 3 shows, performance improvements of 15–26% are possible without recourse to DAD.

As mentioned earlier, Table 2 ( $\lambda=1.642$ ) shows that imperfect structure  $A_i$  passes ASCE 7-02 Standards, which require  $\lambda=1.6$ , but barely. A note of caution must be sounded here: in discussing the wind maps used, ASCE 7-02 states in its commentary (Sect. C6.5.4, p. 275): "It is not likely that the 500-year event is the actual speed at which engineered structures are expected to fail." As the 500-year speed corresponds approximately to the speed that induces allowable stress times the wind load factor, a load factor of 1.6 should not be associated with collapse, according to the ASCE 7 Commentary, that is, the wind loads' margin of safety with respect to collapse should be larger than 1.6. In fact, for the structure analyzed, this is not the case. When initial deformations are accounted for, the structure passes ASCE 7-02 Standards only to the extent that wind load factors specified in the Standards may be construed to be associated closely with collapse or (ultimate) strength design, which requires that "the design strength of each structural component or assemblage shall equal or exceed the required strength based on the factored loads" (AISC 2001, A5.3). This conclusion was only possible when a nonlinear, ultimate analysis was performed. For other structures, nonlinear analysis may reveal even more serious capacity deficiencies. The margin of safety mentioned in ASCE 7-02 Commentary is therefore overly optimistic.

## Discussion and Conclusions

This paper presented an improved version of the NLDAD method for estimating ultimate capacity under wind loads. The paper also showed how NLDAD can be used to substantially increase the safety level of the frame under wind loads with only modest or no increase in material consumption, or save material and energy embodied therein while maintaining wind-resisting capacity. The method consists of using databases of pressures measured in wind tunnel tests and applying these pressures in nonlinear structural analyses. Available databases of experimental measurements provide structural designers with an envelope of peak loads for all critical sections of a structure, that typically are far closer to actual loads than the simplified pressure distributions specified by building codes (Simiu et al. 2003), although in the particular case of the example presented in this paper this was not the case.

To illustrate the method we investigated one frame of a steel warehouse originally designed to satisfy ASCE 7-93 wind loads and ASD requirements. The results of the calculations showed that, for a realistic case where fabrication imperfections are present, the ratio between wind loads under which the ultimate capacity is reached and wind loads inducing allowable stresses (i.e., the wind load factor at ultimate strength) is about 1.6 for loads induced by ASCE 7-02 loads, and about 1.7 for loads obtained from wind tunnel tests. A NLDAD analysis of an improved version of the original design showed that a 3.6% increase in weight results in a 30% increase in the capacity of the frame to resist wind. Conversely, a decrease in weight of up to 10% is possible with NLDAD, with no loss of structural capacity. When initial deformations are accounted for, the structure passes ASCE 7-02 Standards only to the extent that wind load factors specified in the Standards may be construed to transform allowable stress levels to ultimate strength levels, requiring a full plastic analysis.

Our results indicate that, had the frame been designed on the basis of the ASCE 7-02 ASD provisions rather than of the more conservative ASCE 7-93 provisions, its smaller ultimate capacity would have been inadequate. Even for the frame designed in accordance with ASCE 7-93, the effective wind load factor of about 1.6 or 1.7 determined by the NLDAD calculations can hardly be viewed as adequate. Indeed, a load factor of 1.6 corresponds to an estimated nominal mean recurrence interval of the order of 500 years, and therefore to a significant probability of exceedance during a 50-year period.

The Commentary to ASCE 7-02 (Sect. C6.5.4) states: "It is not likely that the 500-year event is the actual speed at which engineered structures are expected to fail, due to resistance factors in materials, due to conservative design procedures which do not always analyze all load capacity, and due to a precise definition of 'failure.'" Our NLDAD analysis suggests that this statement would be overly optimistic if applied in an undifferentiated manner to the type of frame analyzed here, especially in cases where redistribution effects are not significant. Insofar as NLDAD analyses allow estimates of ultimate capacity that are physically more meaningful than the statement in ASCE 7 Commentary Sect. C6.5.4, we believe that it is a step forward and that it has the potential for contributing to the design of safer and/or more economical structures. NLDAD is a form of plastic design as defined in the *AISC Manual*. However, NLDAD is not necessarily proposed for routine office calculations, but rather for calculations intended to develop standards provisions that reflect actual structural capacity more correctly than current methods based

on linear response do. NLDAD could also be warranted for the design of industrialized buildings, due to their importance or because they are mass produced.

## Disclaimers

Certain trade names or company products are mentioned in the text to specify adequately the experimental procedure and software used. In no case does such identification imply recommendation or endorsement by the National Institute of Standards and Technology (NIST), nor does it imply that the equipment or software is the best available for the purpose. The policy of the NIST is to use the International System of Units (SI or metric units) in all its publications. However, in North America in the construction and building materials industry, certain non-SI units are so widely used instead of SI units that it is more practical and less confusing to include customary units as the principal units of measurements, and only customary units in the figures.

## Acknowledgments

This work is part of a long-range research effort conducted by the Structures Group, Building and Fire Research Laboratory, aimed at achieving safer, and more economical steel structures subjected to wind loads. Stimulating exchanges with Emil Simiu are acknowledged with thanks.

## References

- American Institute of Steel Construction (AISC). (1989). *Allowable stress design*, 9th Ed., Chicago.
- American Institute of Steel Construction (AISC). (2001). *Load and resistance factor design specification for structural steel buildings*, 3rd Ed., Chicago.
- American Society of Civil Engineers (ASCE). (1993). *Minimum design loads for buildings and other structures*, SEI/ASCE 7-93, New York.
- American Society of Civil Engineers (ASCE). (2003). *Minimum design loads for buildings and other structures*, SEI/ASCE 7-02, Reston, Va., Chaps. 2 and 6 and Commentary C2 and C6.
- Jang, S., Lu, L. W., Sadek, F., and Simiu, E. (2002). "Database-assisted wind load capacity estimates for low-rise steel frames." *J. Struct. Eng.*, 128(12), 1594–1603.
- Lin, J., and Surry, D. (1997). "Simultaneous time series of pressures on the envelope of two large low-rise buildings." *BLWT-SS7-1997*, Univ. of Western Ontario, London, Ont., Canada.
- Simiu, E., and Miyata, T. (2006). *Design of buildings and bridges for wind*, Wiley, Hoboken, N.J., 127.
- Simiu, E., Sadek, F., Whalen, T. M., Jang, S., Lu, L. W., Diniz, S. M. C., Grazini, A., and Riley, M. A. (2003). "Achieving safer and more economical buildings through database-assisted, reliability-based design for wind." *J. Wind. Eng. Ind. Aerodyn.*, 91, 1587–1611.
- Simiu, E., and Scanlan, R. H. (1996). *Wind effects on structures*, 3rd Ed., Wiley, New York.
- Whalen, T., Shah, V., and Yang, J. S. (2000). "A pilot project for computer-based design of low-rise buildings for wind loads—The WILDE-LRS user's manual." *NIST GCR 00-802*, National Institute of Standards and Technology, Gaithersburg, Md.